**JOURNAL OF THEORETICAL AND APPLIED MECHANICS**
**58**, 4, pp. 853-869, Warsaw 2020
DOI: 10.15632/jtam-pl/125302

# DYNAMIC ANALYSIS OF THE AORTIC VALVE FUNCTIONING

Krzysztof Patralski
*Wroclaw University of Science and Technology, Faculty of Mechanical Engineering, Wroclaw, Poland*
*e-mail: krzysztof.patralski@pwr.edu.pl*

The aim of the paper was to recognize the influence of mechanical factors on the movement of the leaflets. Mechanical stimuli may have a positive effect on remodeling the leaflet material to adapt its structure to a changing load. A model of the valve functioning process was developed. A geometric model similar to the construction of a natural valve was adopted. The hybrid process of the liquid-solid interaction problem was described. The interaction process was modeled. The problem was formulated with the Galerkin FEM method. Numerical analyses of a single valve work cycle and the calcification process of aortic valve bioprostheses were performed.

*Keywords:* aortic valve, algorithm ALE, fluid-structure interaction, finite element analysis

## 1. Introduction

The subject of this study is the aortic valve located at the outflow of the left ventricle. It is made of three spherical leaflets connected by a fibrous ring. The valve leaflet has a composite-layered structure. The orthogonal arrangement of fibers in the layers determines their orthotropic properties. The majority of fibers are arranged in the distinguished radial and circumferential directions. Geometry of individual fibers is the reason that the material shows strongly nonlinear elastic properties. The external layers are a mechanism responsible for transferring loads to other structures during the valve work cycle (Borkowska *et al.*, 2017). During aortic valve functioning, the material undergoes large deformations, reaching up to sixty percent (Ghista and Reul, 1983; Bosi *et al.*, 2018).

The aim of the study was to recognize the influence of mechanical factors on the functioning of the aortic valve. The developed model of the valve functioning allows one to simulate not only the physiological state of the valve but also disease states of the valve leaflet, and thus the disfunction of the entire organ (Chiyoya *et al.*, 2018; Sellaro, 1997; Arzani and Mofrad, 2017).

To model the issue of dynamic flow through the aortic valve, the numerical FEM method was used in the Galerkin formulation. The studied process is a classic issue of the interaction between a fluid and structure (Fluid-Structure Interaction – FSI). In this process, we observe deformations of the shell of the leaflet caused by the flowing liquid, and disturbances of the flow caused by the opening valve (de Hart *et al.*, 2003; Su *et al.*, 2014). The method Arbitrary Lagrangian-Eulerian (ALE) was used. This algorithm requires modification due to the use of two different motion descriptions for the fluid and structure as well as large deformations of the leaflet, which is observed (Gnyaneshwar *et al.*, 2002; Sodhani *et al.*, 2018; Joda *et al.*, 2016).

## 2. Modeling of the aortic valve functioning process

The subject of the research is a material body composed of two continuous areas: the fluid area $\Omega_f$ bounded by the edge $\Gamma_f$ and the area of the solid body (structure) $\Omega_s$ bounded by the edge $\Gamma_s$. Both areas are connected by a border $\Gamma$, an interface between these areas (Fig. 1).

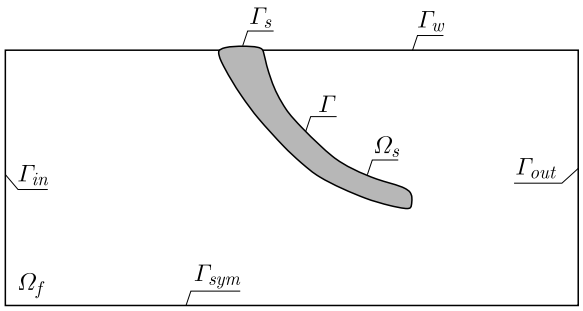


Fig. 1. Analyzed material body

The boundary $\Gamma_f = \Gamma_{in} \cup \Gamma_{out} \cup \Gamma_w \cup \Gamma_{sym}$ is composed of three sub-boundaries: $\Gamma_{in}$ and $\Gamma_{out}$ are respectively the inlet and outlet of the fluid through the valve, $\Gamma_w$ is the boundary of adherence of the fluid to the aorta, and the $\Gamma_{sym}$ is the boundary condition of symmetry of the analyzed problem.

The model of the valve functioning process was formulated by assumptions:

- the material of the $\Omega_s$ area (valve leaflet) is an elastic, homogeneous or orthotropic-fibrous composite body,
- the area of $\Omega_s$ is a shell of constant or variable thickness,
- the $\Omega_s$ area on the edge $\Gamma_s$ is rigidly attached to the aorta,
- the area $\Omega_f$ is a Newtonian or non-Newtonian fluid,
- on the edge of $\Gamma_{in}$ and $\Gamma_{out}$, kinetic boundary conditions (fluid pressure) or kinematic boundary conditions (fluid velocity) are set.

The issue was formulated by writing equations describing the behavior of individual subareas of the fluid and solid as well as the interface surface connecting these two areas. In the model of the fluid area $\Omega_f$, the equation of motion takes the form

$$\rho_f \frac{d\mathbf{v}_f}{dt} = \nabla \cdot \boldsymbol{\sigma}_f + \mathbf{f}_f \tag{2.1}$$

where $\mathbf{v}_f(\widehat{x}^i, t)$ is the vector of velocity, $\boldsymbol{\sigma}_f$ is the Cauchy stress tensor, $\mathbf{f}_f$ is the body force.

By saving the material derivative of the fluid velocity with respect to the spatial coordinate system $\{\chi^i\}$, equation (2.1) can be written in the form

$$\rho_f \Big( \frac{\partial \mathbf{v}_f}{\partial t} + (\mathbf{v}_f - \widehat{\mathbf{v}}) \cdot \nabla \mathbf{v}_f \Big) = \nabla \cdot \boldsymbol{\sigma}_f \tag{2.2}$$

where $\mathbf{v}_f$ is the local velocity of the system $\{\chi^i\}$ moving relative to the fixed spatial coordinate system $\{x_i\}$. It is assumed that the fluid is an incompressible medium, in which case the principle of mass conservation and constitutive equations take the form

$$\nabla \cdot \mathbf{v}_f = 0 \qquad \boldsymbol{\sigma}_f = -p_f \mathbf{I} + \boldsymbol{\tau}_f = -p_f \mathbf{I} + \frac{1}{2}\mu(\nabla \mathbf{v}_f + \mathbf{v}_f \nabla) \tag{2.3}$$

where $\mu$ is the viscosity coefficient, $\boldsymbol{\tau}_f$ is the deviator of the stress tensor, $p_f$ is isotropic fluid pressure.

In the model of the solid area $\Omega_s$, the equation of equilibrium takes form

$$\nabla \cdot \boldsymbol{\sigma}_s + \mathbf{f}_s = \mathbf{0} \tag{2.4}$$

where $\boldsymbol{\sigma}_s$ is the Cauchy stress tensor, $\mathbf{f}_s$ is the body force.

For an incompressible body, the mass conservation equation is in the form

$$\det(\mathbf{F}) - 1 = 0 \tag{2.5}$$

where $\mathbf{F} = \nabla \mathbf{x}$ is the deformation gradient.

The constitutive relation for the incompressible elastic body will be written in the form

$$\boldsymbol{\sigma}_s = -p_s \mathbf{I} + \boldsymbol{\tau}_s \tag{2.6}$$

where $\boldsymbol{\tau}_s$ is the deviator of the stress tensor, $p_s$ is isotropic pressure. Further considerations were made assuming no presence of body forces in the areas $\Omega_f$ and $\Omega_s$.

In the interface model $\Gamma$, on the surface connecting the $\Omega_f$ and $\Omega_s$ areas, the velocity of fluid and solid particles are equal, hence for the points lying on $\Gamma$, the condition must be met

$$v_f = v_s \tag{2.7}$$

The local formulation of the interaction issue can be called a system of equations (2.2)-(2.5) and (2.7) together with definitions (2.6) and appropriate boundary and initial conditions.

## 3. Hybrid description of the fluid-solid interaction problem

From the mechanical point of view, the process analyzed is the interaction between the fluid and structure. In this process, the interaction of two different media is observed: solid and fluid, which model the aortic valve and blood, respectively. Within the framework of mechanics to describe the movement, different Lagrange's and Euler's descriptions are used.

The Lagrange description is used in solid matter problems. The functions of the condition of the material body, in particular motion, deformation and stress state, are functions of material coordinates $\{X^1, X^2, X^3\}$ and time $t$. These functions are related to material points that change their position relative to spatial coordinates during motion $\{x^1, x^2, x^3\}$. Usually, the spatial coordinate system is assumed to be unchangeable over time.

The material derivative with aspect to time of any scalar function $\Phi(X^1, X^2, X^3, t)$ will be saved in the form

$$\frac{d\phi}{dt} = \frac{\partial \phi(X^1, X^2, X^3)}{\partial t} \tag{3.1}$$

Euler's description is used to describe the issues of fluid mechanics. In this case, the functions of the center state are spatial coordinate functions $\{x^1, x^2, x^3\}$ and time $t$. The material derivative on any scalar function $\Phi(x^1, x^2, x^3, t)$ is described in the form

$$\frac{d\phi}{dt} = \frac{\partial \phi(x^1, x^2, x^3, t)}{\partial t} + v_1 \frac{\partial \phi}{\partial x_1} + v_2 \frac{\partial \phi}{\partial x_2} + v_3 \frac{\partial \phi}{\partial x_3} \tag{3.2}$$

where $\{v_i\}$ is a velocity vector.

The material derivative in the Euler description is the sum of the partial time derivative and the convective derivative, where $(v_1, v_2, v_3)$ it is the vector of the fluid velocity at the point $\{x^1, x^2, x^3\}$.

Let us assume that in the interaction problem, for the solid body occupying the $\Omega_s$ area, the Lagrange description is used, and the Euler description is used for the fluid occupying the $\Omega_f$ area. In this case, some duality occurs when formulating the boundary conditions on the common boundary $\Gamma$. Points on the edge $\Gamma$ simultaneously belong to the area of the solid body and the fluid area. In the analytical formulation of conditions for the continuity of kinematic and kinetic fields, the dualism of the formulation does not pose major problems, whereas a significant

problem occurs with the use of FEM, in particular when selecting a discrete model. The geometry of the finite element in the $\Omega_s$ area is immutable relative to the material coordinate system $\{X^1, X^2, X^3\}$, whereas geometry of the finite element in the area $\Omega_f$ is not variable relative to the spatial arrangement $\{x^1, x^2, x^3\}$. In this case, the movement of the edge $\Gamma$ relative to the spatial layout leads to discontinuities of the discrete model on the edge $\Gamma$.

One way out of this situation is to use the ALE algorithm. The idea behind this algorithm is to introduce a new spatial coordinate system $\{\widehat{x}^1, \widehat{x}^2, \widehat{x}^3\}$ that is a fluid reference configuration. It is assumed that the new coordinate system is associated with the spatial coordinate system $\{x^1, x^2, x^3\}$ with the transforming compound

$$\widehat{\mathbf{x}} = \chi(\mathbf{x}, t) \tag{3.3}$$

The coordinate system $\{\widehat{x}^i\}$ is unstable, wherein the change is coupled with the interface motion between the fluid and the solid moving in the fluid. In particular, at the edge $\Gamma$, the velocity of the material points of the solid body with respect to the coordinate system $\{\widehat{x}^i\}$ is zero. Then the grid of discrete models of the fluid and solid on the interface will be continuous if the finite element in the fluid area will be unchanging with respect to the system $\{\widehat{x}^i\}$, and in the initial moment these meshes will have common nodes on $\Gamma$.

We consider the motion of the material point $P$ (Fig. 2) with respect to the spatial coordinate system $\{x^i\}$ in the time interval $(t, t + \Delta t)$. The location of the point changes according to the dependence

$$\mathbf{x}(t) \to \mathbf{x}(t + \Delta t) = \mathbf{x}(t) + \Delta\mathbf{x} \tag{3.4}$$

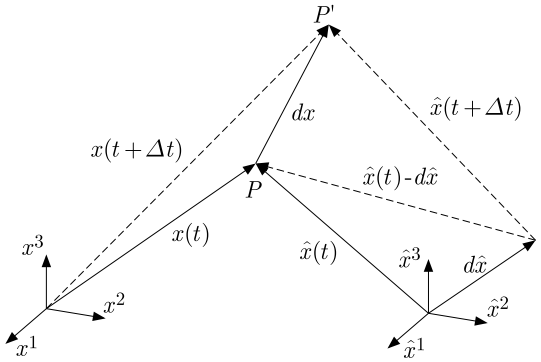


Fig. 2. Kinematic relations for the point $P$ in a spatial system in relation to two reference systems $\{x^i\}$ and $\{\widehat{x}^i\}$

However, if the equation of motion is stored in the moving system $\{\widehat{x}^i\}$, then the change in the position of the $P$ point will be given by the dependence

$$\widehat{\mathbf{x}}(t) \to \widehat{\mathbf{x}}(t + \Delta t) = \widehat{\mathbf{x}}(t) + (\Delta\mathbf{x} - \Delta\widehat{\mathbf{x}}) \tag{3.5}$$

where $\Delta\widehat{\mathbf{x}}$ is the shift of the coordinate system $\{\widehat{x}^i\}$ relative to $\{x^i\}$ at the time $\Delta t$.

Considering the above dependencies, the material derivative of the state function $\phi(\widehat{\mathbf{x}}, t)$ of the material particle $P$ stored in the reference system $\{\widehat{x}^i\}$ is equal to

$$\frac{d\phi}{dt} = \frac{\partial\phi(\chi^1, \chi^2, \chi^3, t)}{\partial t} + (v_1 - \widehat{v}_1)\frac{\partial\phi}{\partial x_1} + (v_2 - \widehat{v}_2)\frac{\partial\phi}{\partial x_2} + (v_3 - \widehat{v}_3)\frac{\partial\phi}{\partial x_3} \tag{3.6}$$

where $(v_i - \widehat{v}_i)$ is the difference in velocity of the material point and the speed of movement of the reference system $\{\widehat{x}^i\}$ relative to $\{x^i\}$. In the ALE method, the fluid problem is defined relative to the reference system $\{\widehat{x}^i\}$.

Due to the large leaflet deformation, the ALE algorithm found in commercial codes requires inclusion of the remeshing procedure to redefine the discrete fluid model. Approximation of nodal parameters in subsequent iterations is necessary, which means that the final parameter values have little accuracy (de Hart *et al.*, 2003). In paper (Chen and Luo, 2018), the immersed boundary method was used. The method is based on decomposition of the computational domain and also requires mesh repair processes. Simulation was able to capture both realistic deformation and structures in the flow, however, we observe a symmetrical process of leaflet buckling, which does not occur in a natural process.

## 4. Formulation of the problem with the weighted residue method

The local formulation described above can be presented in an equivalent form of weak formulation. One of the most general weak formulations is the weighted residue method, which is shown below.

In the area $\Omega = \Omega_f \cup \Omega_s$, the weight functions were selected

$$\phi_{\alpha i}(\mathbf{x}) \in \Phi_\alpha \quad i = 1,2,3,\ldots \quad \alpha = f,s \quad \text{set of linearly independent scalar functions,}$$
$$\psi_{\alpha j}(\mathbf{x}) \in \Psi_\alpha \quad j = 1,2,3,\ldots \quad \alpha = f,s \quad \text{set of linearly independent scalar functions.}$$

The weight functions were selected in the interface area

$$\theta_k(\mathbf{x}) \in \Theta \quad k = 1,2,3,\ldots \quad \text{set of linearly independent scalar functions.}$$

The following definitions of matrix weight functions are accepted

$$\boldsymbol{\varphi}_{\alpha i} = \phi_{\alpha i}\mathbf{I}_3 \quad i = 1,2,3\ldots \quad \alpha = f,s \qquad \boldsymbol{\theta}_k = \theta_k \mathbf{I}_3 \quad k = 1,2,3\ldots$$

where $\mathbf{I}_3$ is the unit matrix of dimension 3.

The weight functions form the complete base of the respective function spaces. Then, the formulation of local issues of interaction with the given system of equations can be replaced with an equivalent system of residual form equations

$$\begin{aligned}
&\int_{\Omega_f} \boldsymbol{\varphi}_{fi} \cdot \left(\rho_f \frac{\partial \mathbf{v}_f}{\partial t} + (\mathbf{v}_f - \widehat{\mathbf{v}}) \cdot \nabla \mathbf{v}_f - \nabla \cdot \boldsymbol{\sigma}_f - \mathbf{f}_f\right) d\Omega + \int_\Gamma \boldsymbol{\varphi}_{fi} \cdot \boldsymbol{\lambda}\, d\Gamma = 0 \qquad \forall \phi_{fi} \in \boldsymbol{\Phi} \\
&\int_{\Omega_f} \psi_{fj}(\nabla \cdot \mathbf{v}_f)\, d\Omega = 0 \qquad \forall \psi_{fj} \in \boldsymbol{\Psi} \\
&\int_{\Omega_s} \boldsymbol{\varphi}_{si} \cdot (\nabla \cdot \boldsymbol{\sigma} + \mathbf{f}_s)\, d\Omega - \int_\Gamma \boldsymbol{\varphi}_{si} \cdot \boldsymbol{\lambda}\, d\Gamma = 0 \qquad \forall \phi_{si} \in \boldsymbol{\Phi} \\
&\int_{\Omega_s} \psi_{sj}(\det(\mathbf{F}) - 1)\, d\Omega = 0 \qquad \forall \psi_{sj} \in \boldsymbol{\Psi} \\
&\int_\Gamma \boldsymbol{\theta}_k \cdot (\mathbf{v}_f - \mathbf{v}_s)\, d\Gamma = 0 \qquad \forall \theta_k \in \boldsymbol{\Theta}
\end{aligned} \tag{4.1}$$

Equations $(4.1)_1$ and $(4.1)_3$ have been introduced into the integral component, in which there is a vector function $\boldsymbol{\lambda}$, which is interpreted as a Lagrange multiplier. This multiplier has a physical interpretation. Equations $(4.1)_1$ and $(4.1)_3$ express the weight residual of the failure of the global equation of equilibrium in the areas $\Omega_f$ and $\Omega_s$, respectively. The boundary is a particular limitation of these areas – it has a variable location and, in addition, the loading

of this edge results directly from the interaction of the adjacent areas. Equation $(4.1)_5$ only provides for the compatibility of displacements of the corresponding points of the area to $\Gamma$, while it does not ensure that the mutual interactions of the areas overlap. Let $p_f$ and $p_s$ denote intensities of the internal edge force (stress vector) loading the $\Omega_f$ and $\Omega_s$ areas on the edge, respectively. Due to the continuity of areas on the $\Gamma$ edge, the difference

$$\boldsymbol{\lambda} = \mathbf{p}_f - \mathbf{p}_s \tag{4.2}$$

should be equal to zero. Because condition $(4.1)_5$ does not ensure that this condition is met, then it should be forced by adding additional components to equations $(4.1)_1$ and $(4.1)_3$. These integrals are the resultants of unbalance boundary forces applied to the $\Omega_f$ and $\Omega_s$ areas analyzed as separated sub-areas of the $\Omega$ area.

The integration was performed by parts of equation component $(4.1)_1$

$$\int\limits_{\Omega_f} \boldsymbol{\varphi}_{fi} \cdot (\nabla \cdot \boldsymbol{\sigma}_f)\, d\Omega = \int\limits_{\Gamma_f} \boldsymbol{\varphi}_{fi} \cdot \mathbf{t}_f\, d\Gamma - \int\limits_{\Omega_f} (\nabla \boldsymbol{\varphi}_{fi})^{\mathrm{T}} : \boldsymbol{\sigma}_f\, d\Omega \tag{4.3}$$

Analogous operation can be performed on the component $\int\limits_{\Omega_s} \boldsymbol{\varphi}_{si} \cdot (\nabla \cdot \boldsymbol{\sigma})\, d\Omega$ from equation $(4.1)_3$. Finally, a new system of equations is obtained instead of a system of equations (4.1)

$$\begin{aligned}
&\int\limits_{\Omega_f} \boldsymbol{\varphi}_{fi} \cdot \Big( l\rho_f \frac{\partial \mathbf{v}_f}{\partial t} + (\mathbf{v}_f - \widehat{\mathbf{v}}) \cdot \nabla \mathbf{v}_f \Big)\, d\Omega + \int\limits_{\Omega_f} (\nabla \boldsymbol{\varphi}_{fi})^{\mathrm{T}} : \boldsymbol{\sigma}_f\, d\Omega + \int\limits_{\Gamma} \boldsymbol{\varphi}_{fi} \cdot \boldsymbol{\lambda}\, d\Gamma \\
&\qquad = \int\limits_{\Omega_f} \boldsymbol{\varphi}_{fi} \cdot \mathbf{f}_f\, d\Omega + \int\limits_{\Gamma_f} \boldsymbol{\varphi}_{fi} \cdot \mathbf{t}_f\, d\Gamma \\
&\int\limits_{\Omega_f} \psi_{fj} (\nabla \cdot \mathbf{v}_f)\, d\Omega = 0 \\
&\int\limits_{\Omega_s} (\nabla \boldsymbol{\varphi}_{si})^{\mathrm{T}} : \boldsymbol{\sigma}_s\, d\Omega + \int\limits_{\Gamma} \boldsymbol{\varphi}_{si} \cdot \boldsymbol{\lambda}\, d\Gamma = \int\limits_{\Omega_s} \boldsymbol{\varphi}_{si} \cdot \mathbf{f}_s\, d\Omega + \int\limits_{\Gamma_s} \boldsymbol{\varphi}_{si} \cdot \mathbf{t}_s\, d\Gamma \\
&\int\limits_{\Omega_s} \psi_{sj} (\det(\mathbf{F}) - 1)\, d\Omega = 0 \qquad\qquad \int\limits_{\Gamma} \boldsymbol{\theta}_k \cdot (\mathbf{v}_f - \mathbf{v}_s)\, d\Gamma = 0
\end{aligned} \tag{4.4}$$

The system of equations contains at most the first derivatives of the state function relative to geometric variables, which is important in construction of the FEM algorithm. The issue was formulated in terms of FEM in the Galerkin version.

## 5. Solution of FEM equation by an increment-iterative method

In order to solve the problem, a generally accepted strategy is adopted, based on formulation of an increment-iterative algorithm for solving the problem in geometric and temporal space. In particular:

a) Solutions are searched in the time interval $(0, T)$ by dividing this interval into equal sections of $\Delta t$. These segments determine on the time axis the time moments $t_0, t_1, t_2, \ldots, t_n, t_{n+1}, \ldots$, where $t_{n+1} - t_n = \Delta t = \text{const}$

b) The solution consists of a sequence of solutions on individual sections of time. The starting point for the time segment $(t_n, t_{n+1})$ is the moment $t_n$ in which the system has reached the dynamic equilibrium, and the vector of nodal parameters is equal $\mathbf{q}_n = \mathbf{q}(t_n)$ and the vector $\mathbf{F}_n = \mathbf{F}(t_n)$. Next, a solution is looked for at the moment $t_{n+1}$ by finding a vector of nodal parameters $\mathbf{q}_{n+1} = \mathbf{q}(t_{n+1})$.

The algorithm for solving the equation by the weighted residual method is presented below. At the time interval $\langle t_n, t_{n+1}\rangle$, the parameter vector is interpolated with the dependency

$$\mathbf{q}(\tau) \approx \widehat{\mathbf{q}}(\tau) = \mathbf{q}_n + \frac{\tau}{\Delta t}(\mathbf{q}_{n+1} - \mathbf{q}_n) \quad \text{where} \quad \tau = t - t_n \tag{5.1}$$

The above interpolation is consistent with the standard linear FEM interpolation, which can be formulated as

$$\widehat{\mathbf{q}}(\tau) = N_n\mathbf{q}_n + N_{n+1}\mathbf{q}_{n+1} = \Big(1 + \frac{\tau}{\Delta t}\Big)\mathbf{q}_n + \Big(\frac{\tau}{\Delta t}\Big)\mathbf{q}_{n+1} \tag{5.2}$$

Substituting (1.32) to (1.28) and calling for resetting of the weighted residuum (weighted error), we have

$$\int_0^{\Delta t} W\big(\mathbf{C}\dot{\widehat{\mathbf{q}}}(t) + \mathbf{K}\widehat{\mathbf{q}}(t) - \mathbf{F}(t)\big)\, d\tau = 0 \tag{5.3}$$

where $W(\tau)$ is a weight function. If enter the weight parameter

$$\theta = \frac{1}{\Delta t}\frac{\displaystyle\int_0^{\Delta t} W\tau\, d\tau}{\displaystyle\int_0^{\Delta t} W\, d\tau} \tag{5.4}$$

then the equation can be written in the form

$$\frac{\mathbf{C}(\mathbf{q_{n+1}} - \mathbf{q}_n)}{\Delta t} + \mathbf{K}\big(\mathbf{q}_n + \theta(\mathbf{q}_{n+1} - \mathbf{q}_n)\big) + \overline{\mathbf{F}} = \mathbf{0} \tag{5.5}$$

where $\overline{\mathbf{F}}$ is the weighted average size over a period of time. We finally obtain

$$\mathbf{q}_{n+1} = (\mathbf{C} + \Delta t\theta\mathbf{K})^{-1}\{[\mathbf{C} - \Delta t(1-\theta)\mathbf{K}]\mathbf{q}_n - \overline{\mathbf{F}}\} \tag{5.6}$$

This scheme depends on the choice of the weight function. The above mentioned problem solving scheme is a first order diagram and gives a numerical error of the order of $0(\Delta t)$.

## 6. FEM algorithm for dynamic analysis of aortic valve functioning

The following is a detailed FEM algorithm used to analyze the valve functioning process. The fluid involved in the process is treated as a Newtonian fluid. The fluid flow through the valve is disturbed by changes in the pressure conditions at the inlet and outlet of the aortic duct, the action of the valve leaflet, and deformation of the aortic wall. In the valve operation process, two areas of the structure and fluid interact with each other. In this work, full mutual interaction between the areas is considered. When formulating the FEM algorithm, the dynamic analysis of the aortic valve used an independent Lagrange and Euler (ALE) description for the structure and fluid area, respectively. An important element of the ALE method is proper adaptation of the discrete FEM model in the fluid area to the time varying position of the discrete FEM structure model. In the case of large displacements, the ALE method leads to degeneration of the mesh, hence the need to modify it. A modified version called ALE-MA was used.

The algorithm for solving the problem of dynamic valve analysis is presented in the form of a block diagram shown in Fig. 3.

In the background of the research, the most suitable geometric valve model was sought. Due to proportions of dimensions, the Reul model (Cacciola *et al.*, 2000) was adopted, which seems to be the closest to the natural valve shape.

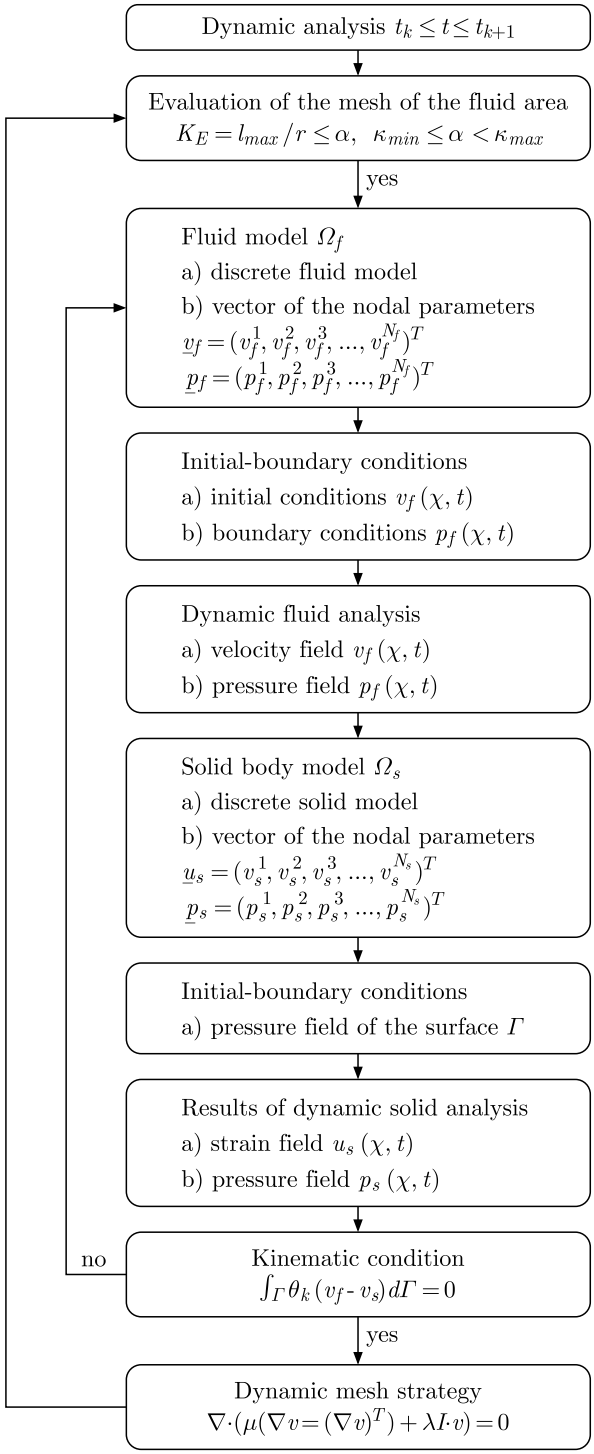


Fig. 3. Fluid-Structure Interaction algorithm

The geometric shape of the aortic valve leaflet has been developed on the basis of measurements of natural leaflets. It was assumed that the cusp is a fragment of the rotational ellipsoid described by the equation (Fig. 4)

$$\frac{x^2}{a_x^2} + \frac{y^2}{a_y^2} + \frac{z^2}{a_z^2} = 1 \tag{6.1}$$

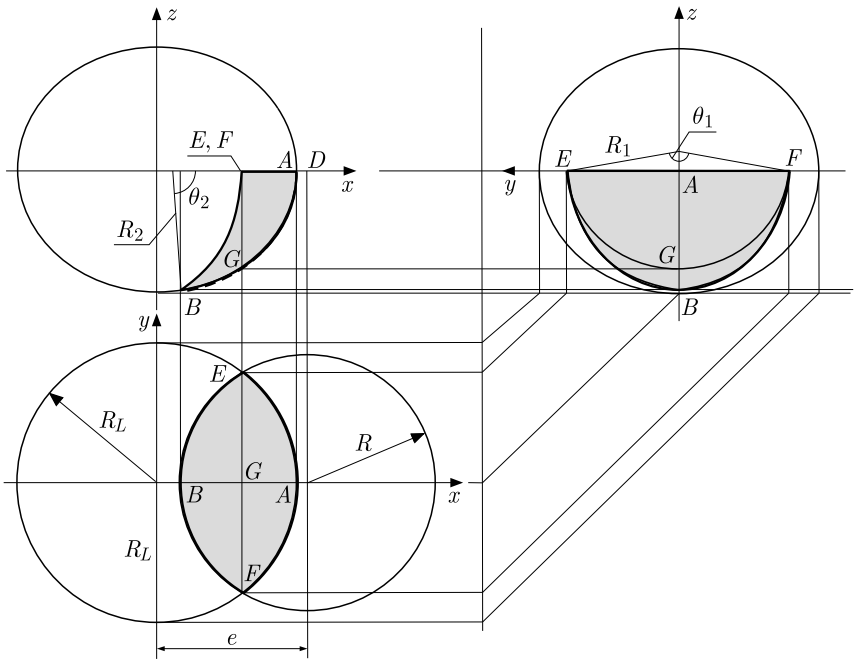


Fig. 4. Geometric model of the Reul valve leaflet

where

$$a_x = a_y = R_L \qquad a_z = \frac{R_L R_2 \sin\theta_2}{\sqrt{R_L^2 - (e-R)^2}}$$

Single leaflet geometries were obtained by cutting an ellipsoid with a circular cylinder with radius equal to the aortic radius and equation

$$\frac{(x-e)^2}{R^2} + \frac{y^2}{R^2} = 1 \qquad \text{and plane} \quad z = 0 \tag{6.2}$$

The Reul geometric model is defined by three parameters: aortic radius $R$, radius of the circumferencial curvature $R_L$ and radius of the radial curvature $R_2$. Model parameters were selected based on measurements of the natural valve leaflets.

Assuming that the three valve cusps are identical and the aorta within the valve is a circular cylinder, the valve is geometrically contained in the segment of the circular cylinder and has six planes of symmetry. When performing analysis of the valve work, the symmetry properties were used, which allowed one to limit the analysis area to a cylinder section containing only one leaflet. Geometric data of valve model elements is shown in Fig. 5, where $R$ is aortic radius, $l_a$ is length of the aortic tube taken as the valve component, $h_k$ is size of the cooptation (leaflets fitting).

When analyzing the valve functioning process, the following specific assumptions are used:

a) The leaflet shell (area $\Omega_s$) is treated as a three-dimensional area with constant thickness $h$. The material is treated as an isotropic hyperelastic body. A five parameter Mooney-Rivlin model was adopted for which the elastic energy density is formulated in the form

$$W = c_{10}(I_1-3)+c_{01}(I_2-3)+c_{20}(I_1-3)^2+c_{11}(I_1-3)(I_2-3)+c_{02}(I_2-3)^2+\frac{1}{d}(J-1) \tag{6.3}$$

where $I_1$, $I_2$ are invariants of the right Green strain tensor, $J$ is the determinant of the deformation gradient, $d$ is the material incompressibility parameter, and $c_{ij}$ coefficients are material constants.

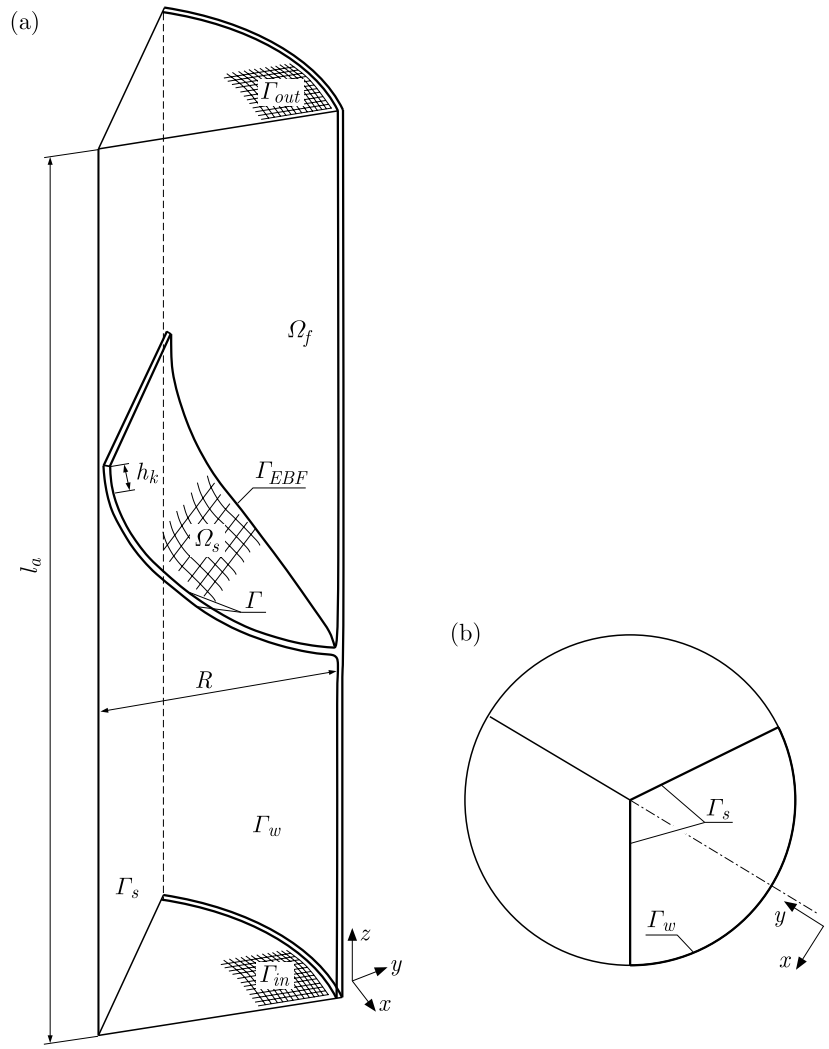


Fig. 5. Analyzed aortic valve fragment, $R = 15\,\text{mm}$, $l_a = 45\,\text{mm}$, $h_k = 3\,\text{mm}$: (a) axonometric view of the fragment of the valve leaflet, (b) view of the whole valve from the aortic axis side with designation of the analyzed fragment

b) The influence of the layered and fibrous structure on the physical properties of the leaflet material is omitted. It is assumed that the strain energy density results from the average properties of the natural leaflet layers of the valve.

c) Blood (area $\Omega_f$) was modeled as a Newtonian liquid characterized by density $\rho$ and the dynamic viscosity coefficient $\mu$. The fluid motion is described by the Navier-Stokes equation and the mass behavior equation

$$\rho\frac{\partial \mathbf{v}}{\partial t} + \rho(\mathbf{v}\nabla)\mathbf{v} = -\nabla p + \mu\nabla^2\mathbf{v} \qquad \nabla v = 0 \tag{6.4}$$

d) Aortic valve leaflet motion is caused by a flowing liquid whose character and flow conditions determine time-varying functions of pressure applied to the edge of the artery $\Gamma_{f1}$.

e) Only the leaflet shell undergoes interaction with the flowing liquid, and the aortic wall is assumed to be non-deformable. It is also assumed that in the initial configuration, the shell is free from stresses. The initial configuration is understood as valve configurations in the closed state at the moment when the pressure is balanced before and after the valve.

f) The aim of the developed ALE-MA algorithm was to improve the analysis of the interaction process by eliminating the remeshing process in the fluid area due to its deformation caused by large displacements of the structure.

## 7. Numerical analysis of a single valve work cycle

The numerical analysis was performed for the area consisting of a single leaflet of the aortic valve surrounded by a fluid. Despite the existence of the axis of symmetry in the presented model, it was decided to analyze the whole leaflet due to the possibility of an asymmetrical form of buckling. At the edge of the shell, appropriate boundary conditions were assumed, taking into account symmetries of the aortic artery.

The following boundary conditions and loading conditions are adopted in numerical calculations:

a) The $\Gamma_{sym}$ area is treated as a non-viscus wall on which the velocity and gradient of fluid velocity in the normal direction to the surface is equal to zero

$$v_y = vy = 0 \qquad \frac{\partial v}{\partial y} = 0 \quad \text{on} \quad \Gamma_{sym} \tag{7.1}$$

b) The aortic wall $\Gamma_w$ is treated as a viscous wall on which the velocity of the fluid is equal to zero

$$v_x = v_y = v_z = 0 \quad \text{on} \quad \Gamma_w \tag{7.2}$$

c) The leaflet on the edge $\Gamma_s$ is rigidly attached to the aorta, which expresses the boundary conditions in the form

$$u_x = u_y = u_z = 0 \quad \text{on} \quad \Gamma \tag{7.3}$$

d) The pressure field is a function of time on the inlet $\Gamma_{in}$ and outlet $\Gamma_{out}$ surface of the aortic duct. The load was based on actual measurements of the heart cycle.
e) During the process, the fluid exerts pressure load over time on both ventricular and aortic surfaces of the leaflet. The ventricular and aortic surfaces of the leaflet shell constitute the $\Gamma$ interface, which is treated as a viscous wall boundary.
f) The SST (Shear Stress Transport) algorithm was chosen to describe the turbulent flow. It is a model based on the concept of Reynolds averaged equations (RANS).

Studies of the natural aortic valve were performed on the ultrasound (USG) measurements. Natural valve tests were performed in a two-dimensional projection.

## 8. Results

The process of opening the valve model starts with the deviation of the free edge of the leaflet towards the wall of the artery (Figs. 6a,b). Next, we observe motion of the whole shell and, in particular, its central part towards the wall of the vessel. The process of loss of stability of the leaflet shell begins, which in a short period of time experiences a large deformation (Figs. 6c,d). The place of initiation of this process is located in the axis of symmetry of the shell near the place of its attachment to the wall of the artery. As a result of full opening of the valve, the free edge of the shell is corrugated, which in the final stage of the valve opening process takes a shape of an arch, which is typical for natural valves.

The flow through the valve continues until the pressure difference between the $\Gamma_{in}$ surface (ventricle) and the $\Gamma_{out}$ surface (aortic artery) remain. When pressure on the surface $\Gamma_{in}$ reaches a value lower than pressure prevailing on the surface $\Gamma_{out}$, the process of closing the valve begins. In the initial phase, a return of the free edge of the leaflet is observed towards the axis of the artery (Fig. 6f). Then, due to the inflow of the fluid onto the outflow part (aortic) of the shell, it buckles in the direction of the vessel axis closing the valve (Figs. 6g,h). When the valve closes, there is a small backflow.

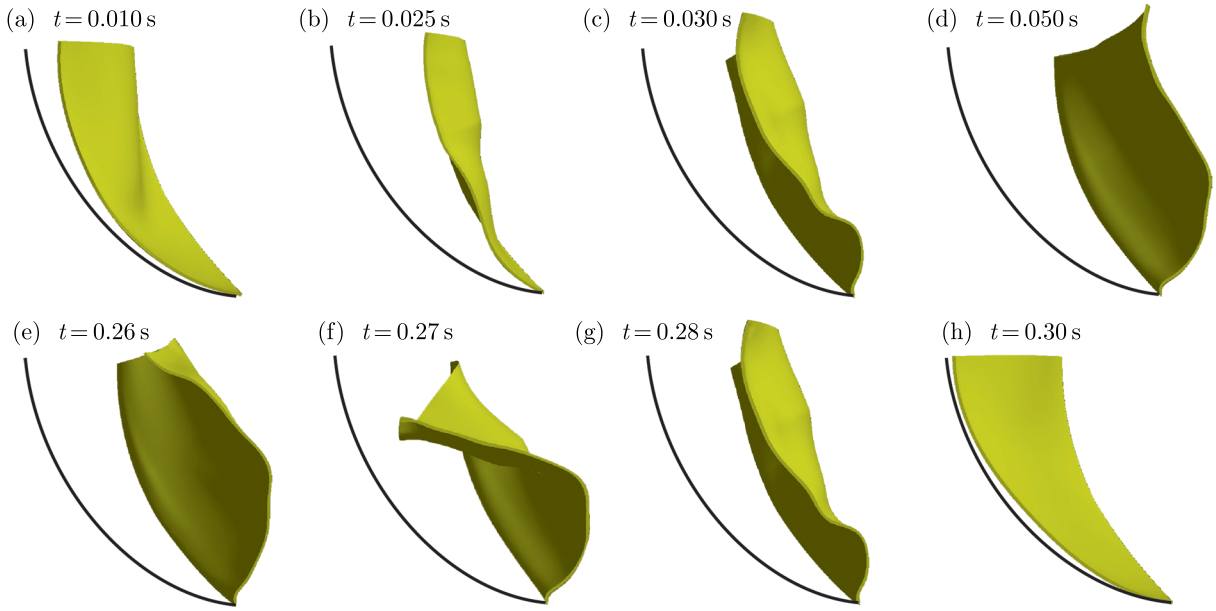


Fig. 6. Deformation of the leaflet model. Projection perpendicular to the plane of symmetry of the leaflet

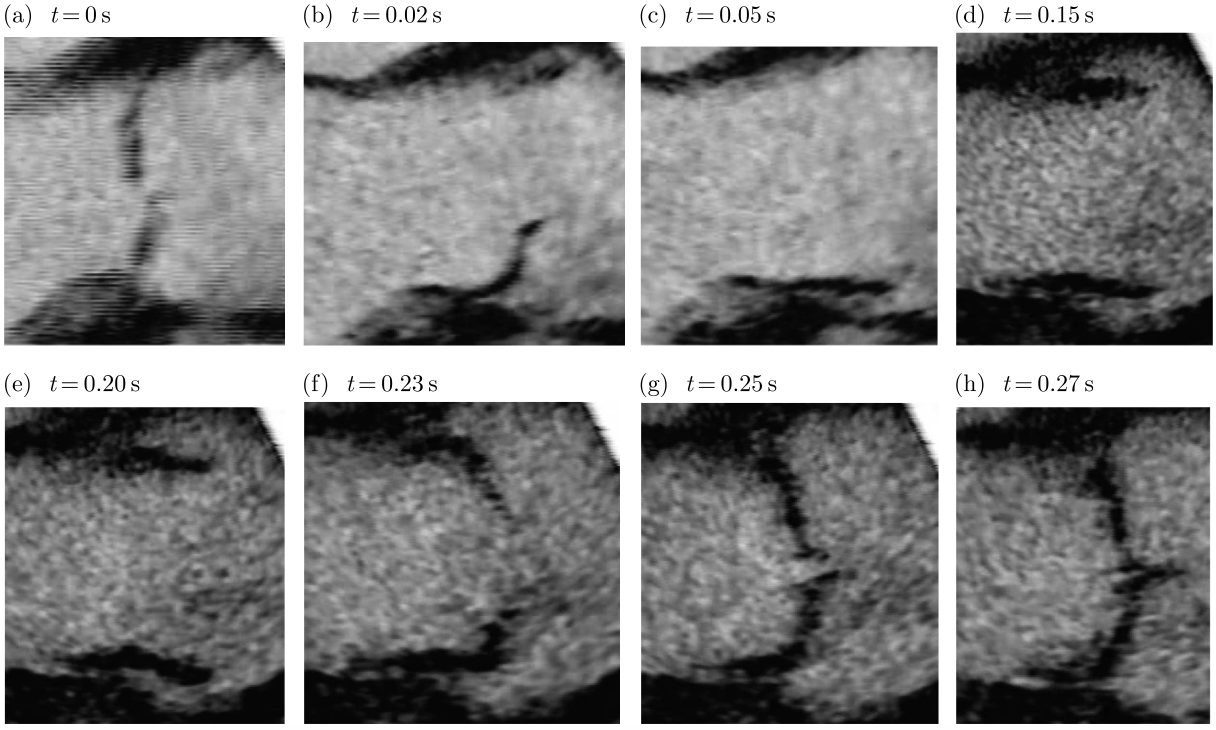


Fig. 7. Deformation of the natural leaflet. Projection perpendicular to the plane of symmetry of the leaflet

Natural leaflet deformations are shown in Fig. 7. Figure 7b shows the moment of loss of stability of the leaflet shell and of directing the free edge of the shell to the axis of the vessel. Figure (7c-e) shows the open valve. The leaflets inclined towards the wall of the artery ensure a correct opening field of the valve. Figure 7f shows the initial stage of the closing of the valve, when we observe the direction of the free edge of the leaflet towards the axis of the vessel, then buckling the leaflet and closing the valve (Figs. 7g,h).

The deformation process of the leaflet model and natural leaflet is determined by the pressure conditions prevailing at the interface between the fluid and the structure in the fluid flow through the valve. The configuration of deformation states is different in the process of opening and closing of the valve. In the analysis of both objects, the moment of shell stability loss was revealed. The process of natural leaflet deformation and the model are similar.

Analyzing the model deformation process in the projection perpendicular to the plane of the aorta cross-section, it is observed that in the initial phase, when the free edge of the coating deviates towards the vessel wall, the deformation state is asymmetrical (Fig. 8a). In subsequent time periods, the deformation process and growth of the open field are symmetrized until the circular shape is reached by the free edge of the coating (Fig. 8d). This is a characteristic process for natural valves. The process of closing the valve model in the described projection is characterized by gradual reduction of the opening area until the valve is completely closed.

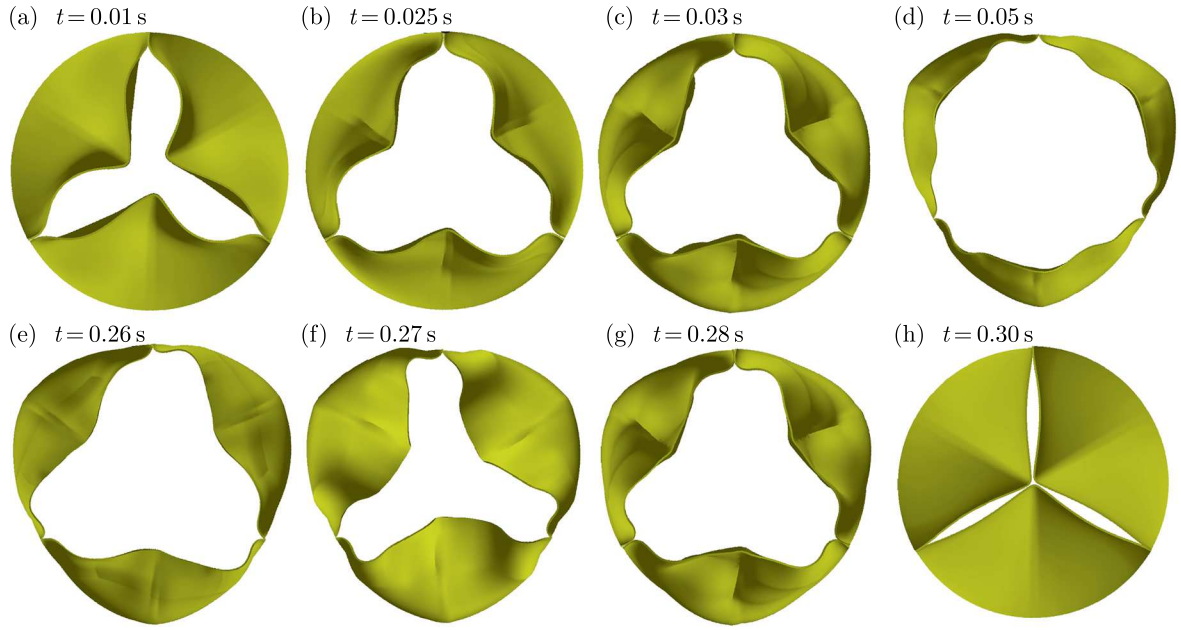


Fig. 8. Deformation of the leaflets of the valve model. Projection perpendicular to the plane of the aorta cross-section

The description of the opening process of the valve model presented is similar to the process of opening the natural valve. Figure 9b shows the asymmetrically deviated free edges of the leaflet, and then the moment of loss of stability of the shell (Fig. 9c). A progressive opening process of the valve was observed until the opening field was reached (Figs. 9d-9f). In the case of a natural valve, we observed a similar process (Figs. 9g-9l).

The obtained image of the native aortic valve functioning in ultrasound measurements has been confirmed in numerical modeling. Ghista and Reul (1983) presented results of numerical analysis of the valve model interaction process. The results concerning the deformation analysis correspond with the results presented in this work. In vivo tests carried out by this team confirm the convergence of deformation states configurations in which the leaflet shell undergoes with the results presented in the paper.

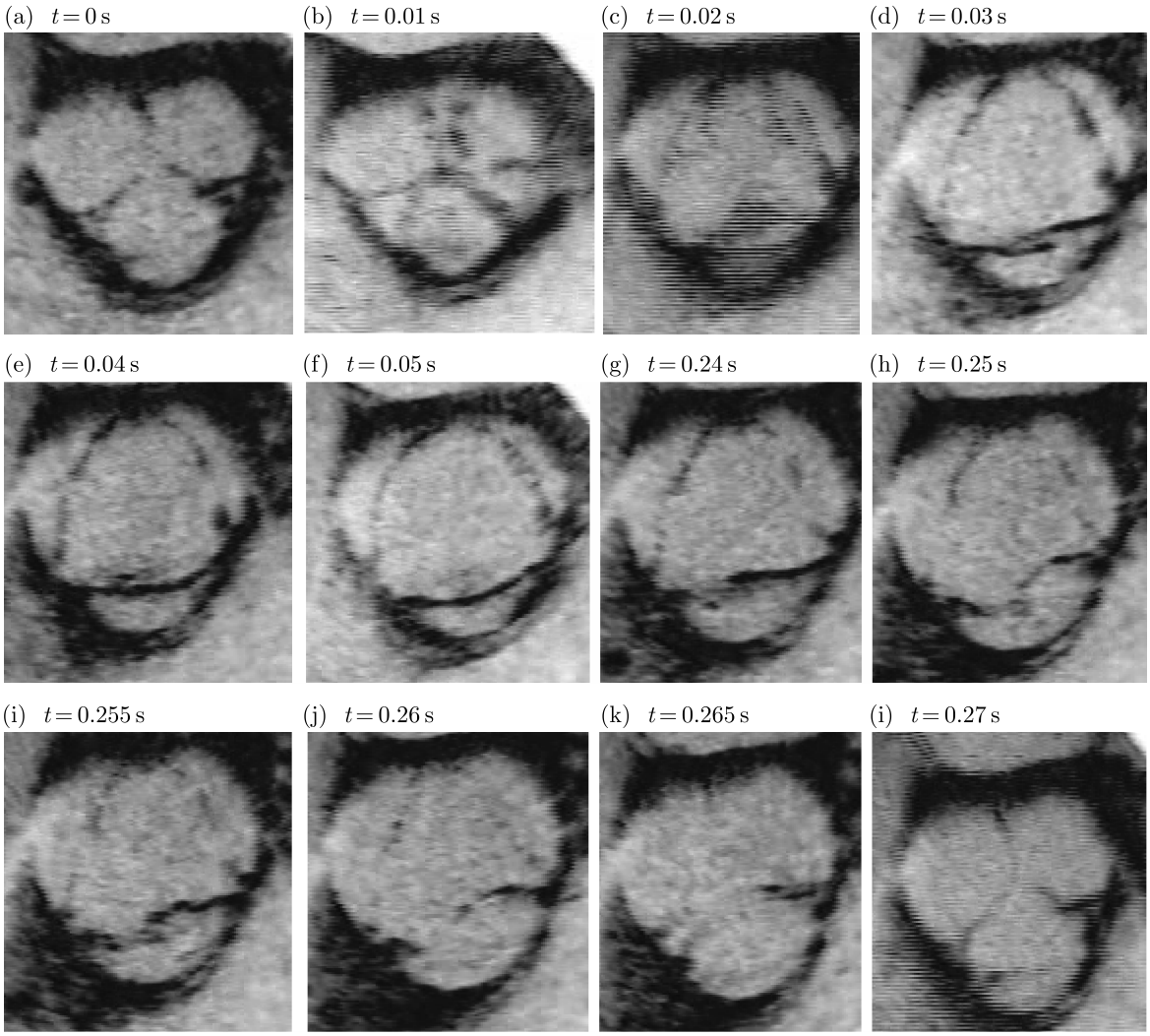


Fig. 9. Deformation of the leaflets of the natural valve. Natural projection to the plane of the cross section of the aortic artery

The dependence of the change in the opening area of the natural valve and the model is shown in Fig. 10. The parameter which often differs in the experiments described in the work on aortic valve modeling work is the working time of the tested object. It consists of: time of valve opening phase $t_s$, period in which the valve remains open $t_t$, closing time of the valve $t_z$.

During the ejection of the fluid towards the ventricular surface, we observe an increasing axial flow (Figs. 11a,b) and flow in the aorta bulb caused by the leaflets movement toward the vessel wall (Fig. 11c). As the load increases, the progressive deformation of the leaflets increases the opening area of the valve. Figures 11d and 11e show the state of loss of stability and the associated intensification of flow. A central flow was observed in the axis of the aorta. The fluid stream is separated and a vortex forms. In the further part of the artery, the flow stabilizes. At the final stage of ejection, pressure is equalized on both sides of the valve, and then lowers on the ventricular surface $\Gamma_{in}$ below the pressure in the aorta $\Gamma_{out}$. As a result of changes in the boundary conditions, the flow direction is reversed (Fig. 11g). The fluid flowing to the surface of the aortic leaflet causes the feedback process of dislocating the leaflet from the configuration after buckling to the natural configuration which, in effect, causes the valve to close (Fig. 11h). During the closing process, a small backflow occurs (Fig. 11i).

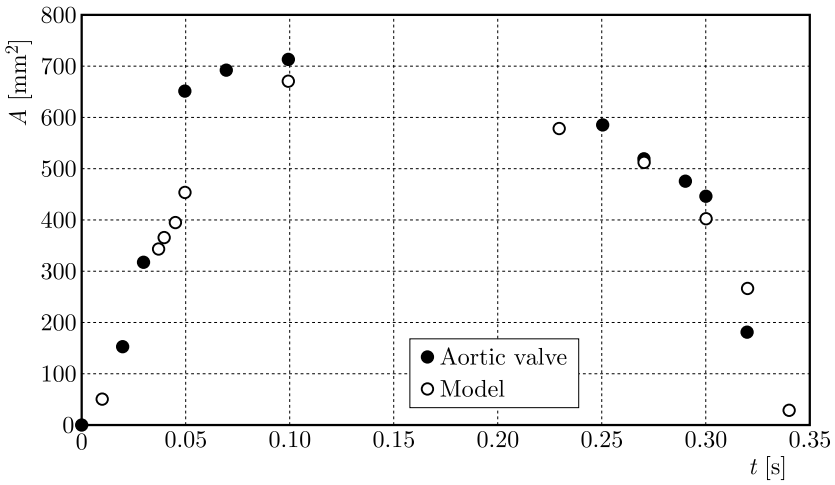


Fig. 10. Dependence of the change in the opening area of the natural valve • and the model ○ as a function of time

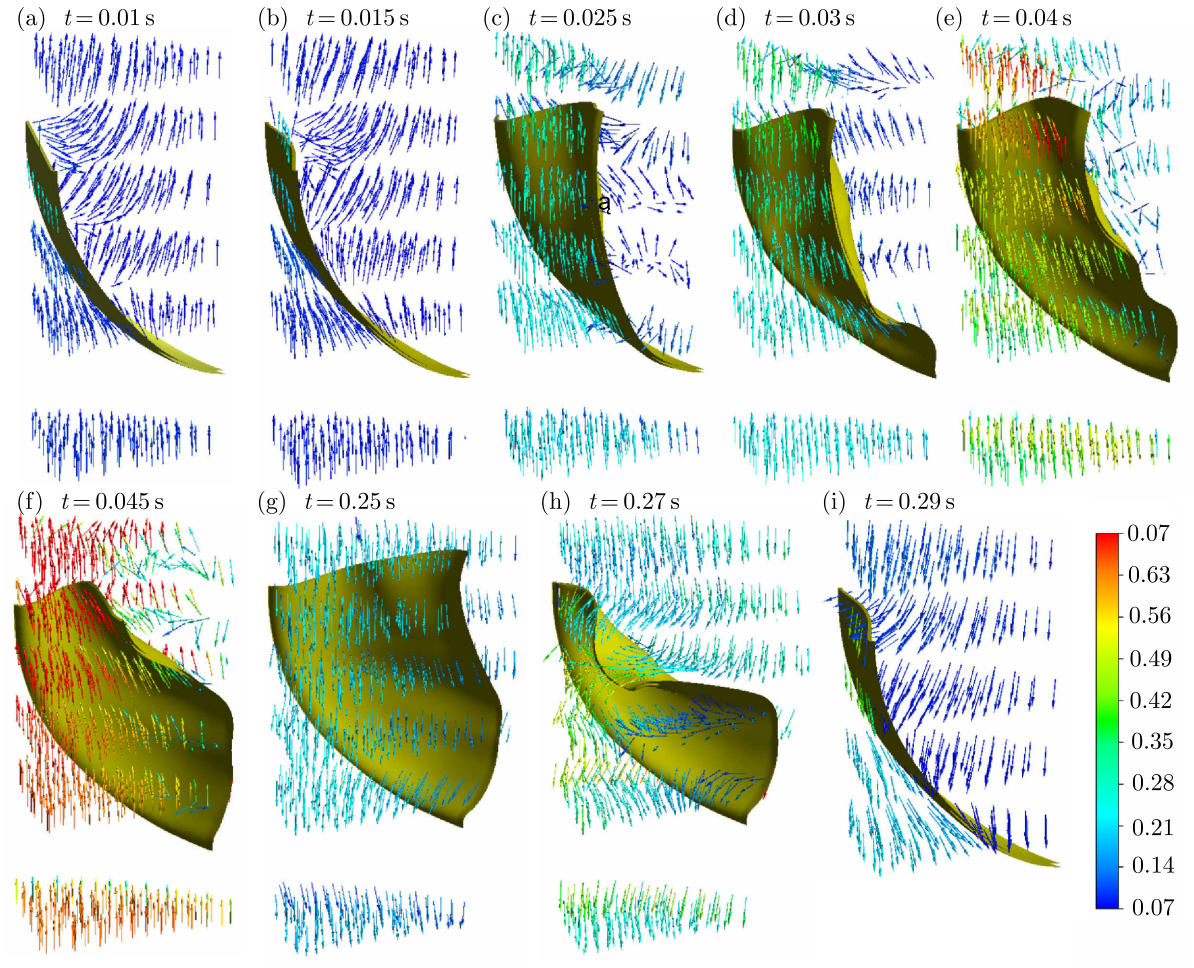


Fig. 11. Distribution of the velocity field

The maximum velocity obtained in the modeled process was $v_{max} = 0.70\,\mathrm{m/s}$. The Reynolds number Re for velocity $v_{max}$ was 6300, and the Strouhal number St = 0.037. In the real flow, the maximum velocity $v_{max} = 0.82\,\mathrm{m/s}$ was obtained, the Re = 7380, and St = 0.031.The dynamics of the flow through the valve indicates laminar-turbulent nature of the flow. During the flow

around the leaflet, we observed the formation of a vortex structure in the space. A similar phenomenon was described in (Joda *et al.*, 2016). The results are confirmed by the velocity values obtained in the USG measurements.

## 9. Discussion

In (Chen and Luo, 2018), the process of deformation of the aortic leaflet model is similar to the results obtained by the author. The similarity applies especially to the phase when the valve is closed and discontinuities of the cusps contact are visible (Fig. 8h). However, there are doubts in the symmetrical deformation process, which is asymmetrical in the model presented in the paper as well as in the natural process (Fig. 9h). This is due to some imperfections in the construction of the leaflet shell.

Chen and Luo (2018) showed the moment of leaflet buckling, which is similar to the results of the author. The difference occurs only at the time when the buckling occurs due to different duration of the valve work cycle. The mentioned differences in the parameters of the heomdynamic process and differences in the selection of the valve size had an impact on the parameters obtained in the paper (Chen and Luo, 2018), i.e. valve opening area, which was $1.67\,\mathrm{cm}^2$, volume flow and flow velocity. However, similar vortex structures were observed around the leaflet during valve opening and closing.

In papers (Gnyaneshwar *et al.*, 2002; de Hart *et al.*, 2003), the velocity fields were presented. The similarity of the vortex structures flowing around the cusp shell and the central stream of the fluid occurring during the ejection phase of the blood from the left ventricle is noticeable. In both works, a similar average blood ejection velocity through the valve $v \simeq 1\,\mathrm{m/s}$ was recorded.

The numerical tool presented in the paper allows modeling the fluid-structure interaction process. This algorithm enables modeling of the functioning bioprostheses. It allows one to assess the influence of geometrical parameters of the leaflet on the hemodynamic parameters of the entire valve. The solution allows modeling the character of the flow around the valve cusp and analyzing the formation of stagnation zones. Within this solution, it is possible to analyze the reasons for the development of the calcification process, which is the most destructive process of the currently used bioprostheses.

## References

1. Arzani A.M., Mofrad M.R.K., 2017, A strain-based finite element model for calcification progression in aortic valves, *Journal of Biomechanics*, **65**, 216-220

2. Borkowska A.M., Nowakowski M., Lis G.J., Wehbe K., Cinque G., Kwiatek W.M., 2017, Molecular structure of human aortic valve by $\mu$SR-FTIR microscopy, *Nuclear Instruments and Methods in Physics Research Section B: Beam Interactions with Materials and Atoms*, **411**, 129-135

3. Bosi G.M., Capelli C., Cheang M.H., Delahunty N., Mullen M., Taylor A.M., Schievano S., 2018, Population-specific material properties of the implantation site for transcatheter aortic valve replacement finite element simulations, *Journal of Biomechanics*, **71**, 236-244

4. Cacciola G., Peters G.W.M., Baaijens F.P.T., 2000, A synthetic fiber-reinforced stentless heart valve, *Journal of Biomechanics*, **33**, 653-658

5. Chen Y., Luo H., 2018, A computational study of the three-dimensional fluid-structure interaction of aortic valve, *Journal of Fluids and Structures*, **80**, 332-349

6. Chiyoya M., Seya K., Yu Z., Daitoku K., Motomura S., Imaizumi T., Fukuda I., Furukawa K.-I., 2018, Matrix Gla protein negatively regulates calcification of human aortic valve

interstitial cells isolated from calcified aortic valves, *Journal of Pharmacological Sciences*, **136**, 4, 257-265

7. De Hart J., Peters G.W.M., Schreurs P.J.G., Baaijens F.P.T., 2003 A three-dimensional computational analysis of fluid-structure interaction in the aortic valve, *Journal of Biomechanics,*, **36**, 103-112
8. Ghista D.N., Reul H., 1983, Prosthetic aortic leaflet valve design: performance analysis of an avcothane leaflet valve, *Advance Cardiovascular Physiology*, **5**, 31-42
9. Gnyaneshwar R., Kumar R.K., Balakrishnan K.R., 2002, Dynamic analysis of the aortic valve using a finite element model, *The Annals of Thoracic Surgery*, **73**, 1122-1129
10. Joda A., Jin Z., Haverich A., Summers J., Korossis S., 2016, Multiphysics simulation of the effect of leaflet thickness inhomogeneity and material anisotropy on the stress-strain distribution on the aortic valve, *Journal of Biomechanics*, **49**, 12, 2502-2512
11. Sellaro T., 1997, *Effects of Collagen Orientation on the Medium-Term Fatigue Response of Heart Valve Materials*, George Washington University
12. Sodhani D., Reese S., Aksenov A., Soğanci S., Jockenhövel S., Mela P., Stapleton S.E., 2018, Fluid-structure interaction simulation of artificial textile reinforced aortic heart valve: Validation with an in-vitro test, *Journal of Biomechanics*, **78**, 52-69
13. Su B., Zhong L., Wang X.-K., Zhang J.-M., Tan R.S., Allen J.C., Tan S.K., Kim S., Leo H.L., 2014, Numerical simulation of patient-specific left ventricular model with both mitral and aortic valves by FSI approach, *Computer Methods and Programs in Biomedicine*, **113**, 2, 474-482

*Manuscript received October 16, 2019; accepted for print January 29, 2020*